Volume 52 | Number 2 | 7 January 2016 | Pages 217–420

ChemComm

Chemical Communications

www.rsc.org/chemcomm

ISSN 1359-7345

ROYAL SOCIETY OF CHEMISTRY

FEATURE ARTICLE

E. Maisonhaute *et al.*

Transient electrochemistry: beyond simply temporal resolution

175 YEARS

ChemComm

FEATURE ARTICLE

View Article Online
View Journal | View Issue

Cite this: *Chem. Commun.*, 2016, 52, 251

Transient electrochemistry: beyond simply temporal resolution

X.-S. Zhou,[a] B.-W. Mao,[b] C. Amatore,[c] R. G. Compton,[d] J.-L. Marignier,[e] M. Mostafavi,[e] J.-F. Nierengarten[f] and E. Maisonhaute*[g]

Received 22nd September 2015,
Accepted 6th November 2015

DOI: 10.1039/c5cc07953e

www.rsc.org/chemcomm

Some physicochemical intrigues for which transient electrochemistry was necessary to solve the problem are summarized in this feature article. First, we highlight the main constraints to be aware of to access to low time scales, and particularly focus on the effects of stray capacitances. Then, the electron transfer rate constant measured for redox molecules in a self-assembled monolayer configuration is compared to the conductance measured through the same systems, but at the single molecule level. This evidences strong conformational changes when molecules are trapped in the nanogap created between both electrodes. We also report about dendrimers, for which a short electrochemical perturbation induces creation of a diffusion layer within the molecule, allowing the electron hopping rate to be measured and analyzed in terms of molecular motions of the redox centers. Finally, we show that transient electrochemistry provides also useful information when coupled to other methodologies. For example, when an ultrasonic field drives very fast movements of a bubble situated above the electrode surface, the motion can be detected indirectly through a modification of the diffusion flux. Another field concerns pulse radiolysis, and we describe how the reactivity (at the electrode or within the solution) of radicals created by a radiolytic pulse can be quantified, widening the possibilities of electrochemistry to operate in biological media.

Introduction

In any physicochemical method the temporal resolution is an issue, because at each stage, new phenomena are evidenced. In electrochemistry, the measurement timescale is intimately linked to the diffusion processes that occur in the vicinity of the electrode.[1,2] The race for accessing short times was initiated so as to characterize heterogeneous electron transfer kinetics or transient radicals. The different strategies to solve that purpose may be classified in two main categories. In the first one, the size of a stationary diffusion layer δ is controlled finely by the technique. The characteristic timescale t_{char} is then derived simply using eqn (1):

$$t_{char} = A\frac{\delta^2}{D} \quad (1)$$

Here, A is a proportionality parameter that depends on the technique and D is the diffusion coefficient. Such approaches cover the rotating disk electrode[1] or other hydrodynamic methodologies[3] where the diffusion layer is imposed by convection. They also include the use of micro or nano-electrodes in the steady state[4] or the more recent scanning electrochemical microscopy (SECM) configuration.[5] The great advantage of

[a] *Key Laboratory of the Ministry of Education for Advanced Catalysis Materials, Institute of Physical Chemistry, Zhejiang Normal University, Jinhua, Zhejiang 321004, China*
[b] *State Key Laboratory of Physical Chemistry of Solid Surfaces, College of Chemistry and Chemical Engineering, Xiamen University, Xiamen 361005, Fujian, China*
[c] *CNRS UMR 8640 PASTEUR, Ecole Normale Supérieure-PSL Research University, Département de Chimie, Sorbonne Universités - UPMC University Paris 06, 24, rue Lhomond, 75005 Paris, France*
[d] *Department of Chemistry, Physical and Theoretical Chemistry Laboratory, University of Oxford, South Parks Road, Oxford OX1 3QZ, UK*
[e] *Laboratoire de Chimie Physique, CNRS UMR 8000, Université Paris-Sud, Bat 350, 91405 Orsay Cedex, France*
[f] *Laboratoire de Chimie des Matériaux Moléculaires, Université de Strasbourg et CNRS, Ecole Européenne de Chimie, Polymères et Matériaux (ECPM), 25 rue Becquerel, 67087 Strasbourg Cedex 2, France*
[g] *Sorbonne Universités, UPMC Univ Paris 06, UMR 8235, Laboratoire Interfaces et Systèmes Electrochimiques, F-75005 Paris, France. E-mail: emmanuel.maisonhaute@upmc.fr*

Emmanuel Maisonhaute obtained his doctoral degree at the Ecole Normale Supérieure (Paris, France) under the supervision of Christian Amatore in 2000. After a postdoctoral work with Richard Compton (University of Oxford, United Kingdom) during 2000–2001, he returned to Paris as an assistant professor in the group of Christian Amatore and was promoted full professor in 2008. In 2010, he moved to the Laboratoire Interfaces et Systèmes Electrochimiques at Université Pierre et Marie Curie (Paris). He received the Instrumentation Prize of the French Chemical Society in 2008 in recognition for his scientific contributions in ultrafast electrochemistry. His research aims at coupling electrochemical detection to other physicochemical methods.

these approaches is that the double layer charging currents do not interfere with the measurements. In addition, for SECM, the feedback process provides an enhanced sensitivity, up to the single molecule level.[6] Since SECM also allows surface modification and imaging, this technique has quickly become extremely popular far beyond the electrochemical community. However, in SECM a redox mediator is usually needed to shuttle the information between the studied surface and the probe.

The second strategy, to which belong the examples depicted in this paper, involve direct time-dependent perturbations. The prominent methods are cyclic voltammetry,[2] chronoamperometry,[7,8] impedance spectroscopy[9] and their variations. However, applying a short perturbation does not warrant an effective access to lower time scales.[10] This is evidenced considering the simplified electric scheme of an electrochemical interface displayed in Fig. 1. This scheme contains the solution resistance R_S, which depends on the solution composition and electrode geometry, the double layer capacitance C_{DL} that takes into account compensation of the electrode charge by the ions from the solution and the faradaic impedance Z_F. Z_F is a very complex impedance that incorporates the mechanism which needs to be elucidated. The cell time constant τ is defined by:

$$\tau = R_S C_{DL} \quad (2)$$

Whatever the method, the temporal resolution cannot be lower than τ. Furthermore, the current I becomes larger when the timescale diminishes and consequently ohmic losses $R_S I$ introduce an interdependence between the capacitive and faradaic components so that in addition to a lower faradic/capacitive currents ratio, complex mechanisms are more difficult to resolve. With ohmic drop compensation systems, these drawbacks are canceled, allowing complex mechanisms to be more easily analyzed but the temporal resolution is still limited by τ. In this context using small electrodes represents a significant advantage. Considering the prominent disk geometry, R_S is given by:

$$R_S = \frac{\rho}{4r_0} \quad (3)$$

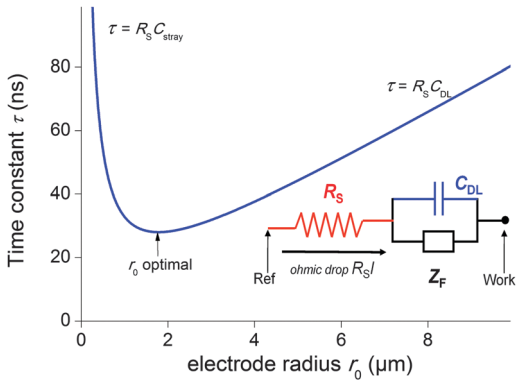

Fig. 1 Simplified electric scheme of an electrochemical interface featuring the solution resistance (red), the double layer capacitance (blue) and the faradaic impedance (black). Blue curve: evolution of the time constant $\tau = R_S C_{global}$ as a function of the electrode radius r_0 when the stray capacitances are not negligible (see text).

where ρ is the solution resistivity and r_0 the electrode radius.[11] Since for short times both the current I and C_{DL} scale with r_0^2, it ensues that $R_S I$ and $R_S C_{DL}$ both scale with r_0. This represents one of the great advantages of using ultramicroelectrodes. During the last century, the temporal resolution in cyclic voltammetry was then progressively improved using different strategies, with or without ohmic drop compensation, by using smaller and smaller electrodes.[12–19] Finally, in 2000, Amatore *et al.* achieved scan rates ν up to 2.5×10^6 V s^{-1} with a 100% ohmic drop compensation, which translates into a temporal resolution of about 20 ns.[20–22] The electrode radius was 2.5 μm.

Therefore, one may be tempted to use nanoelectrodes which are routinely accessible presently to perform even faster measurements. But before, the capacitance of the whole system needs to be reevaluated. As a representative example, let us consider a capacitance per surface area of C_{surf} = 10 μF cm^{-2} and r_0 = 2.5 μm so that the double layer capacitance is only about 2 pF. Such small value stresses that for very small electrodes the global capacitance C_{global}, incorporating all stray components C_{stray} from the electrochemical cell and electronic board of the potentiostat needs to be considered:

$$C_{global} = C_{DL} + C_{stray} = C_{surf}\pi r_0^2 + C_{stray} \quad (4)$$

With this more realistic expression, τ now can be reformulated as:

$$\tau = (\rho C_{surf}\pi r_0)/4 + (\rho C_{stray})/(4r_0) \quad (5)$$

Fig. 1 represents τ as a function of r_0 considering C_{stray} = 1 pF. This representation emphasizes the deviation from the ideal behavior as the electrode radius diminishes. Under these conditions, the best temporal resolution is reached at an optimal radius of 1.8 μm given by:

$$r_0 = (C_{stray}/(\pi C_{surf}))^{1/2} \quad (6)$$

With ρ = 0.1 Ω m, τ = 28 ns. For smaller electrodes, the capacitance is dominated by the defects of the system so that there is no benefit in using nanoelectrodes for achieving direct low time scale measurements.[4] This stresses that an extreme care should be taken when implementing the electronic board of the potentiostat and fabricating the working ultramicroelectrode to minimize C_{stray}.

Overall, though transient and steady state methodologies rely on similar concepts, some systems require a specific technique to unravel the mechanism. For example, all time dependent systems definitely require transient measurements. Also, even if in theory SECM may attain nanosecond timescales, in practice to the best of our knowledge no extremely fast electron transfer rate have been measured.

In this review, we will focus onto some aspects of our research solved through the very good temporal resolution of our potentiostat. The first section will aim at comparing the results obtained by ultrafast cyclic voltammetry and single molecule measurements through the same molecular systems. Then, we will show how diminishing the experimental timescale provides unique information about electron hopping

between the different redox centers of a single macromolecule. We will end this review by describing how the coupling of transient electrochemical measurements (mainly at constant potential) with other transient methodologies such as acoustic cavitation and pulse radiolysis provides useful information about very complex physicochemical mechanisms induced by non-electrochemical perturbations.

Electron transfer through electroactive molecules: transient *versus* single molecule approaches

The dream of molecular electronics would be to build an entire signal processing unit only with molecules. But to be competitive with top down methodologies, several problems need to be considered. First, the molecular design should allow a function. It has been now demonstrated that molecules are indeed able to treat electrical, optical or even magnetic information. This has been demonstrated mostly by relying onto experiments performed on collection of molecules. Another problem is related to the individual organization of each structure. In this aspect, it is now common to organize some nanoobjects over several hundreds of nanometers (the limitation often comes from the substrate) but usually the same entity is assembled.[23,24] Moreover, these organizations often rely on weak interactions so more robust structures need to be produced for practical applications.

The first property to be tested was the ability of a single molecule to propagate a signal, *i.e.* to act as a molecular wire. This can be performed by placing an electron donor and an acceptor at each end of a linear entity and inducing a photochemical activation or pulse radiolysis. For example, this was thoroughly studied in peptides[25] or in DNA[26] but also in many other molecular wires.[27]

In electrochemistry, the donor or the acceptor can be replaced by an electrode. Then, the measured quantity is the heterogeneous standard rate constant k_{ET}.[1,2] Several experimental protocols are available to deduce this parameter, and among them transient ones such as chronoamperometry and ultrafast voltammetry are rather straightforward. The theoretical framework to interpret the evolution of k_{ET} with the potential E has been initially introduced by Marcus.[28] Later, Chidsey proposed a formulation particularly adapted for electroactive self-assembled monolayers that takes into account the Fermi distribution of electronic levels in the electrode:[29]

$$k_{ET}(E) = \frac{\rho\pi^{5/2}H^2}{h}\left(\frac{k_B T}{\lambda}\right)^{1/2} \times \int_{-\infty}^{+\infty} \frac{\exp\left(\left(x - \frac{\lambda \pm e(E - E^{0\prime})}{k_B T}\right)^2 \times \frac{k_B T}{4\lambda_{ox}}\right)}{1 + \exp(x)} dx \quad (7)$$

where $E^{0\prime}$ is the standard potential, H the electronic coupling, ρ the density of states in the electrode and λ the reorganization energy (including internal and solvent coordinates) involved in the electron transfer reaction. In the integral, the $\pm$ sign should be replaced by $-$ for an oxidation and by + for a reduction. The standard rate constant k^0_{ET} is obtained when applying $E = E^{0\prime}$. At low overpotentials $|E - E^{0\prime}|$, an exponential dependence with the potential is recovered so that Marcus and the more classical Butler–Volmer formulations are equivalent.[30] In eqn (7), the coupling factor H reflects the electronic interaction between the redox center and the electrode. On a large number of systems, it was demonstrated that it depends exponentially on the distance d between the redox center and the surface so that:[27]

$$k^0_{ET} = k^0_{ET}(d = 0)\exp(-\beta d) \quad (8)$$

Returning to molecular electronics, the ideal molecular wire would then have a very small β.[31] This indeed occurs with conjugated backbones whereas for alkyl chains β is on the order of 10 nm^{-1}. For long molecular wires, or when several redox centers are present, electron hopping needs also to be considered (see below).

Another more recent approach to test the conduction through molecular wires consist of connecting single molecules between two electrodes. The quantity measured is then the conductance G through the molecule, a steady-state value.[32] In this approach, the benefit is that single entities are addressed, but no temporal resolution has been until now investigated. Several experimental configurations are available, but those deriving from the scanning tunneling microscope break junction (STMBJ) that emerged from 2003, and presently implemented in several groups, are the only ones that allow performing measurements under electrochemical conditions.[33–37] For that, a metallic STM tip, most often a gold one, is insulated so as to minimize the leakage current. It is then approached towards a surface modified with the molecule of interest until contact. During retraction, successive plateaus are observed, each one corresponding to a definite number of molecules contacted between both electrodes.

In the framework of superexchange, theoretical equivalence between conductance measurements through a bridge and electron transfer from an electrode to a redox center separated from the electrode by the same bridge has been examined by several authors and reinforce the intuitive idea that electron transfer rate constants should be correlated to single molecule conductance.[38–40] Like k^0_{ET}, G indeed depends onto H according to:

$$G = \frac{4\pi^2 e^2}{h} H^2 \rho^2 \quad (9)$$

where e is the elementary charge. Nevertheless, when a redox system is connected at both ends, the situation may be different. A pioneer theoretical development has been developed recently by Ulstrup and Kuznetsov.[41,42] The key points are graphically displayed in Fig. 2. The two electrodes are considered as electron reservoirs into which the electrons are distributed according to a

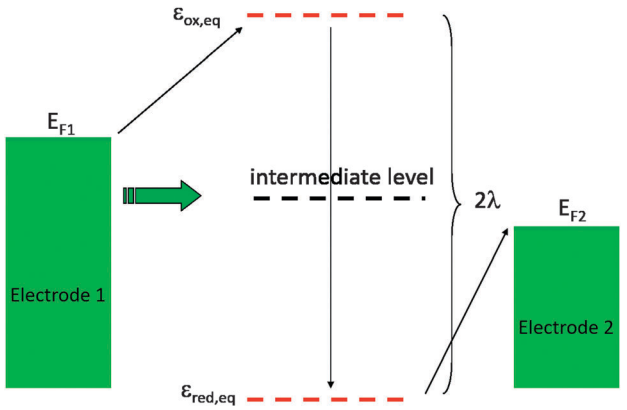

Fig. 2 Energy levels distribution. Green: level distribution in the electrodes. Red: energy levels at equilibrium. Black: intermediate level corresponding to out of equilibrium situation that can transiently efficiently couple both electrodes.

Fermi–Dirac distribution, the electrode potentials setting the two Fermi levels. In the gap, the redox levels of the oxidized (Ox) and reduced (Red) states fluctuate with typical amplitudes given by the reorganization energy λ. These levels are electronically coupled to the electrodes so that electron hopping from the electrodes to or from the redox center may occur. Whether in the relaxation this level passes through both Fermi levels, the electronic coupling is greatly enhanced so that several electrons may tunnel directly between both electrodes. A current maximum is predicted when the sample potential gets close to the standard potential. Small deviations due to the potential profile in the junction may be expected. But to the best of our knowledge, only very few experimental illustration of the above depicted theory have been published.[43,44] Most often, a monotonous variation is observed, suggesting strong conformational changes of the molecule inside the nanogap.

In this context, we tried to explore and relate k^0_{ET} to the conductance G onto the three very different electroactive molecules **1–3** displayed in Fig. 3.[45] Molecules **1–3** differ widely by the nature of their redox center, bridging unit and metal-contacting atoms but have similar size (about 1.9 nm).

The first probe **1** was an Osmium^{II} bisterpyridine complex that may be reversibly oxidized to Os^{III}. Fig. 3 presents cyclic voltammograms at different scan rates obtained for **1** onto gold ultramicroelectrodes. At low scan rate ($<10\,000$ V s^{-1}), the peaks are almost symmetric and bell-shaped because the Os^{III}/Os^{II} ratio follows the equilibrium distribution given by the equilibrium potential (Nernst law). As the scan rate increases, the peak potentials shift because the kinetic window, proportional to Fv/RT is fast enough to compete with k^0_{ET}. k^0_{ET} is then easily deduced by fitting the peak to peak difference with reference curves obtained numerically. For that complex, $k^0_{ET} = 2.0 \times 10^6 \pm 0.5 \times 10^6$ s^{-1} was deduced.

Molecular conductances were determined by the STMBJ method. Fig. 4 presents typical conductance curves obtained when the sample was set at -0.3 V per Pt (pseudo reference

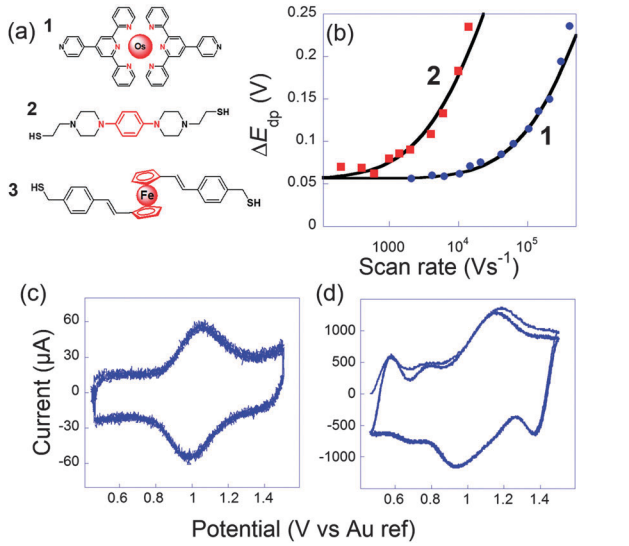

Fig. 3 (a) Molecules **1**, **2** and **3** used to perform ultrafast and single molecule measurements. (b) Peak to peak potential differences obtained for **1** (blue dots) and **2** (red squares). Black lines: simulations for $k^0_{ET} = 2.0 \times 10^6$ s^1 (**1**) and 7×10^4 s^{-1} (**2**). (c and d) Cyclic voltammograms of **1** at (b) 10 400 V s^{-1} and (c) 407 000 V s^{-1}, three consecutive scans, no average. Electrolyte: H_2O + 1 M $NaClO_4$. Adapted from ref. 45.

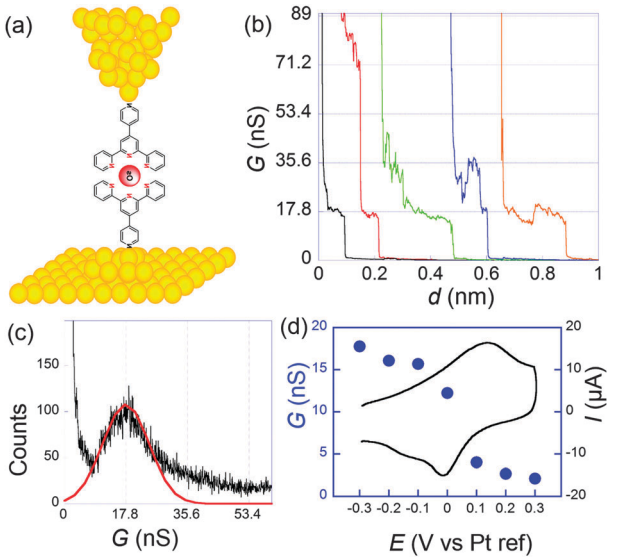

Fig. 4 (a) Schematization of a scanning tunneling microscopy break junction experiment. (b) A few conductance traces obtained for **1** at a sample potential of -0.3 V per Pt and a bias of 50 mV. Electrolyte: 0.1 M $NaClO_4$ aqueous solution. (c) Histogram obtained from the selection of 211 out of 1000 conductance traces. (d) Filled circles: molecular conductance *versus* sample potential. Black line: cyclic voltammogram. Adapted from ref. 45.

electrode). Under these conditions, from statistical analysis of a large number of curves (Fig. 4c), an average single molecular conductance of 17.8 nS was determined. Furthermore, the sample potential was varied from -0.3 to 0.3 V while the bias remained fixed at 50 mV to cover the whole electroactivity range of the complex. This evidenced a clear modulation of the

conductance by the redox switching from 17.8 nS at −0.3 V to 2.1 nS at +0.3 V, which provides an on-off ratio of 8.5 (Fig. 4d).

System **2** conversely contains saturated parts in the bridges, so that the redox center is better isolated from the electrodes. As a consequence the rate of electron transfer was found much slower: $k^0_{ET} = 7 \times 10^4\ s^{-1}$. Since the resistance was higher, we observed more noise in the conductance curves, and it was harder but nevertheless possible to observe well-defined steps. From the resulting histograms constructed at different potentials, we deduced that the conductance shifts from 0.79 nS in the reduced state to 0.33 nS in the oxidized one. Modulation by the potential is thus smaller than for **1** but still appreciable. It has to be underlined that for thiol–gold bonds, several microscopic configurations of the contacts leading to different conductances have been evidenced.[46–48] Here, we refer to the so-called "high conductance" for which the sulphur contacts three gold atoms since we believe this is the most stable configuration, thus closer to the one obtained in self-assembled monolayers.

For system **3**, single molecule conductance was measured at reduced (−0.1 V), oxidized (+0.4 V) and intermediate (+0.2 V) redox states. Very surprisingly, the molecular conductance remained almost unchanged with potential, at a value close to 9.4 nS. The high conductivity was in agreement with the one determined previously in a mechanically controlled break junction experiment without potential control (9.7 nS).[49] The conductance invariance observed for **3** severely contrasts with the behavior of systems **1** and **2** and with any other redox molecules that have been reported so far. Onto similar systems, and in agreement with indirect laser induced temperature jump measurements performed by Chidsey *et al.*,[31] we previously confirmed that the rate constant was nearly independent of the molecular length, as long as redox centers are accessible to counterions. k^0_{ET} was about $5 \times 10^6\ s^{-1}$ for this family.[50]

In the theoretical framework provided by Kuznetsov and Ulstrup,[41,42] the absence of any current maximum near the standard potential indicates a "soft-gating" configuration. As a consequence, the redox levels somehow escape to be in between the Fermi levels of the electrodes. They however still play a role in the coupling so that variations are observed when the sample potential is modified. Here, a potential variation modulates the coupling factor H but the mechanism still remains a superexchange. This demonstrates that large conformational fluctuations occur in the nanogap. It is noticeable that the larger on/off current ratio is higher for the more rigid system **1**. In the extending nanogap more degrees of freedom may be available for flexible molecules so that the situation may thus greatly differ from the behaviour in single component type of self-assembled monolayer where the molecules are well-organized. We then relied on the superexchange framework to evaluate the coupling factor between both electrodes.[38]

The coupling factors H were evaluated for a range of reasonable reorganization energies. Results are reported in Fig. 5. For ferrocene and phenylene diamine derivatives λ is in the range 0.6–1 eV. No reported value exists for **1**, but it may be expected to fall in the same range. For system **3** we obtain an

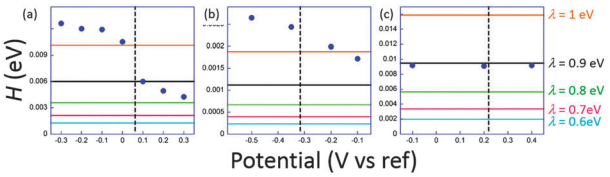

Fig. 5 Estimated electronic coupling elements from conductance measurements (filled circles) and from ultrafast voltammetry (horizontal lines) for a range of reorganization energies ranging from 0.6 to 1 eV for **1** (a), **2** (b) and **3** (c). Vertical dashed line indicates standard potential. Potential scale refers to Pt for (a) and (b), and to SCE for (c). Adapted from ref. 45.

excellent agreement for λ = 0.9 eV, a very plausible value for ferrocenyl derivatives. However, in the junction, reorganization energies can reach smaller values than when the redox centers are fully accessible to solution. This may be correlated to the invariance of k^0_{ET} with the molecular length. For **1** and **2**, H obtained at low potentials in the STMBJ configuration, therefore in the situation for which the self-assembled monolayer is created, is clearly higher than the value deduced by ultrafast voltammetry. Since electron transfer operates over a longer distance in the conductance mode, this result is rather surprising, particularly for **2** whose redox center is connected through long saturated bridges. A possible explanation involves a preferential conformation in the nanogap for which the conductance would be very high compared to the relaxed one for which cyclic voltammetry is performed. This phenomenon has been demonstrated by temperature dependence measurements for dithioalkyls in the gas phase.[51] Conformational changes may be induced by the current itself, or by the tip movement while or after the contact is established. A softer method to realize the contact could minimize the molecular fluctuations and lead to a better correlation. Recent evolutions of the STMBJ technique should allow scrutinizing this issue by allowing conductance measurements at various nanogap width (thus at different molecular conformations) and solve this issue.[52] These results, and particularly those for **3**, although showing a qualitative correlation between k^0_{ET} and G enlightens the need for further theoretical and experimental insights to fully understand the performances of complex molecular systems. It also emphasizes the need for independent and complementary experimental methods to estimate molecular devices performances and usefulness.

Electron hopping within giant molecules

When redox centers are too far from the electrode, H may be too small to drive efficient communication with the surface. However, when several redox centers are present in the molecule, successive electron transfers may occur so that finally the electrochemical perturbation may reach entities placed at several nanometers from the surface. This is the way Nature transfers electrons in many proteic systems such as hydrogenases,[53] and is also debated for DNA.[26,54] In electrochemistry, electron hopping was initially considered by Dahms and

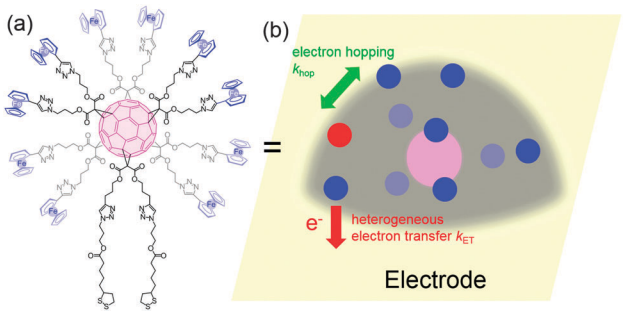

Fig. 6 Molecular formula (a) and schematization (b) of **C_{60}Fc** adsorbed onto an ultramicroelectrode.

Ruff[55,56] and later studied onto polymers by Saveant *et al.*[57] We explored electron hopping in various dendrimer systems and developed an adequate theory to understand the signal propagation within these structures.[58–63] In comparison to polymers, these macromolecules present the advantage to be monodisperse and to form well-defined monolayers. When adsorbed onto electrodes, such compounds can be schematized as truncated spheres onto which are positioned the redox entities.[59] For example, let us consider the system **C_{60}Fc** bearing 10 electroactive ferrocene entities represented in Fig. 6.

With this geometry, we considered that only the redox centers adjacent to the electrode surface may undergo electron transfer from the electrode. Then, intramolecular electron exchanges (the electron hopping steps) occur through:

$$Fc_{site1} + Fc_{site2}^{+} \leftrightarrows Fc_{site1}^{+} + Fc_{site2} \quad (10)$$

We have demonstrated that this behavior may be described by a diffusion of electrons (or symmetrically holes) onto the truncated sphere. The equivalent diffusion coefficient D_{hop} is proportional to the electron exchange rate k_{hop} according to eqn (11):

$$D_{hop} = \frac{2k_{hop}}{3\pi d N_A} \quad (11)$$

where d is the diameter of the ferrocene redox centers and N_A the Avogadro number. However, the redox sites under consideration are here covalently fixed at the surface of the dendrimer so that only small motions around their stable positions are possible. In this view, the problem becomes similar to thin layer cell voltammetry, but the layer is here a nanometric molecular layer. Thus, if cyclic voltammetry is carried out in a low scan rate regime compared to the one corresponding to the propagation of the electrochemical perturbation over the whole molecule, all the Fc metal centers of each adsorbed molecule are oxidized into Fc^+ within one voltammetric scan, so that the voltammogram is that of an adsorbed monolayer. Hence, the current is proportional to ν as for usual self-assembled monolayers.

On the other hand, if the scan rate is fast enough, the diffusion layer extension (δ), becomes smaller than the dimension of the molecule, and a semi-infinite diffusion response is expected. This translates into a $\nu^{1/2}$ dependence of the current. By careful consideration of this sort of diffusional response,

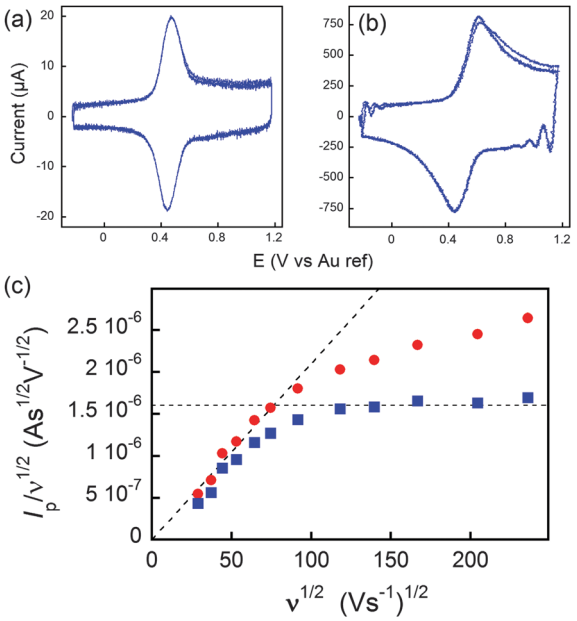

Fig. 7 (a and b) Voltammograms of **C_{60}Fc** at 836 (a) and 55 850 V s^{-1} (b) in acetonitrile +1 M tetra-*n*-butylammonium tetrafluoroborate. (c) Peak current evolution with the scan rate. Red dots: experimental data. Blue dots: corrected data featuring a diffusion plateau at large scan rates. Adapted from ref. 62.

information can furthermore be gained about the topology of the space in which the diffusive process occurs, giving insight into whatever deformation of the dendrimer, if any, takes place upon adsorption to an electrode surface. The transition between both regimes may then be evidenced by plotting $I/\nu^{1/2}$ *versus* $\nu^{1/2}$.

In Fig. 7, at low ν, the current is proportional to ν. However, departing from the cases we previously analyzed, at larger ν a diffusional tail appears in the voltammogram and the slope diminishes but does not reach a plateau as expected. In our view, some redox centers very close to the electrode remain independent, thus keeping a contribution proportional to ν. From the slope ratios, we deduced that two redox centers out of ten were independent. The analysis of the eight centers that were interacting together revealed that D_{hop} spanned the range 1.9×10^{-9} cm^2 s^{-1} < D_{hop} < 1.3×10^{-8} cm^2 s^{-1} so that k_{hop} was deduced to be 3.3×10^5 L mol^{-1} s^{-1} < k_{hop} < 2.2×10^6 L mol^{-1} s^{-1}. This value may be compared to the one deduced by NMR line broadening or stop flow methods pertaining for the self exchange between two independent ferricinium and ferrocene in close contact: $k_{SE} = 7.3 \times 10^6 \pm 0.3 \times 10^6$ L mol^{-1} s^{-1}. Our values are then smaller compared to the one in which the redox centers are touching each other. However, considering that the ferrocene entities are pinned at the apex of an icosahedron, and taking 10 nm^{-1} as minimum value for β since electron transfer occurs through the solvent, we estimated that 2.9×10^2 < k_{pin} < 4.0×10^3 L mol^{-1} s^{-1}. This value is much smaller than k_{hop}, which suggest that molecular motion favors electron transfer, but that the linking chains restrain the electroactive entities mobilities so that k_{pin} < k_{hop} < k_{SE}.

Considering that the redox centers were in a harmonic well, k_{hop} can then be expressed as:

$$k_{hop} = k_{pin} \exp(2\beta x) \exp\left(-\frac{\kappa x^2}{k_B T}\right) \quad (12)$$

where κ is the stiffness constant of the harmonic spring. In eqn (12), the first exponential term stems from the distance dependence of electronic coupling while the second one takes into account the diminished probability of finding a redox entity away from its equilibrium position. Eqn (12) reveals an optimal position corresponding to a situation for which the hopping probability is large enough whereas there is still an appreciable population despite the increased elastic energy. A stiffness constant ranging from $1.9 \times 10^{-2} < \kappa < 9.1 \times 10^{-2}$ J m^{-2} was deduced.

Dendrimer ultrafast electrochemistry represents to the best of our knowledge the first example for which dynamic interactions between redox centers inside single macromolecules could be deciphered. Somehow, we evidenced similar concepts to those relevant to Förster resonance energy transfer approaches in photophysics.[64,65] On the other hand, elucidating the charge propagation in these structures is a pre-requisite prior incorporating them in (opto)electronic devices.

Ultrafast detection of acoustic bubble movement

Another original application of ultrafast electrochemistry concerns the detection of a fast moving object thanks to the perturbation induced on the flux of electroactive material towards an electrode.[66] The resulting signal is then a convolution between the movement and the diffusion layer evolution. The original example considered below demonstrates how extremely fast moving speeds can be detected by transient electrochemistry. Here, electrochemistry acts as a nanometric zoom to indirectly visualize the evolution of the interface.[67–70]

When ultrasound is applied to a solution, for example using a ultrasonic horn, the cohesive forces of the liquid may be overcome when the acoustic pressure exceeds a threshold value. Gas-filled bubbles then grow, especially near inhomogeneities such as solid impurities, surface kinks or tiny gas bubbles. In solution, subsequent evolution varies from oscillating behavior for moderate acoustic pressures to transient one for larger ones. Very high local temperatures and pressures can thus be achieved. Those may be beneficial for electrosynthesis or electroanalysis since the bubbles clean the electrode surface and accelerate greatly the mass transport.[71,72] A common thought previous to our work was that near a surface the implosion of the bubble was asymmetric leading to a toroidal bubble through which a microjet impacted the surface. In fact, this microjet has been observed for large bubbles stimulated at low frequencies[73] or for cavities produced by a laser pulse,[74] thus under very different conditions than those applied usually in sonochemistry,[74] *i.e.* at frequencies ranging from 20 kHz up to 1 MHz. We used our ultrafast electrochemical equipment

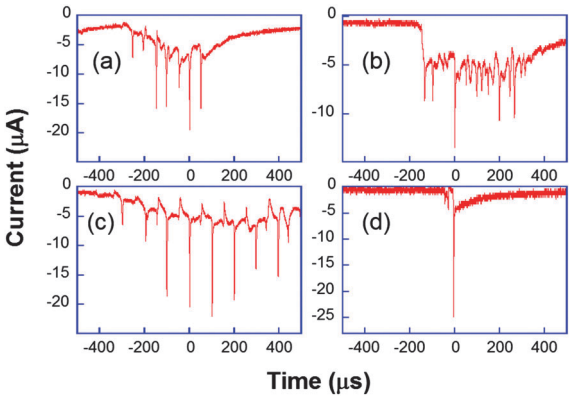

Fig. 8 Chronoamperometric current obtained for the reduction of $K_3[Fe(CN)_6]$ (50 mM) in aqueous KNO_3 under ultrasound power of 8.9 W cm^{-2} at a 29 μm diameter platinum electrode. Horn-to-electrode distances are 10 mm (a–c) and 1 cm (d). Adapted from ref. 67.

and ultramicroelectrodes to visualize indirectly a single bubble evolution through the current induced by its movement.[67,68] Firstly we considered chronoamperometry at a single electrode where $[Fe(CN)_6]^{3-}$ is continuously reduced to $[Fe(CN)_6]^{4-}$, with the electrode held at −0.8 V *versus* a platinum pseudoreference. Fig. 8 shows typical chronoamperograms for a 29 μm diameter platinum electrode under insonation.

Fig. 8a–c are different transients obtained under the same conditions. The observed peaks are attributed to cavitational bubble activity in the vicinity of the electrode. The local acoustic pressure can be increased by reducing the horn-to-electrode separation and a transition is observed from stable towards transient cavitation (see Fig. 8d). Otherwise, the current measured when no bubble was close to the electrode was much higher than the spherical diffusion-limited current under silent conditions. Since it was found to be proportional to the electrode area for a range of electrode diameters, this was attributed to macroscopic acoustic streaming, which leads to a convection-dominant response. Returning to the chronoamperograms, it is obvious that the entire millisecond signal cannot be described as a single peak as suggested elsewhere.[75] Fig. 8 shows that the signal comprises many thin spikes whose rise time can be much less than one microsecond. In some cases, these narrow spikes can be periodic with a frequency of 10 or 20 kHz (Fig. 8c and a, respectively), leading to larger currents that can be up to 200 times higher than the steady-state diffusion-limited current under silent conditions. Higher harmonics of the driving frequency can also be observed (see Fig. 8b).

Complementary experiments by fast scan cyclic voltammetry were performed. In Fig. 9, the cavitation peak is preceded by a long depletion in the voltammetric current, indicating the presence of an obstacle to the diffusion layer growth.

Analogous behaviour was observed with scan rates as high as 10^4 V s^{-1} or even in the capacitive current as displayed in Fig. 9b and d. This suggests that the bubble grows in the close vicinity of the electrode surface: after the spike, the end of the voltammogram overlays with the silent voltammogram, as does

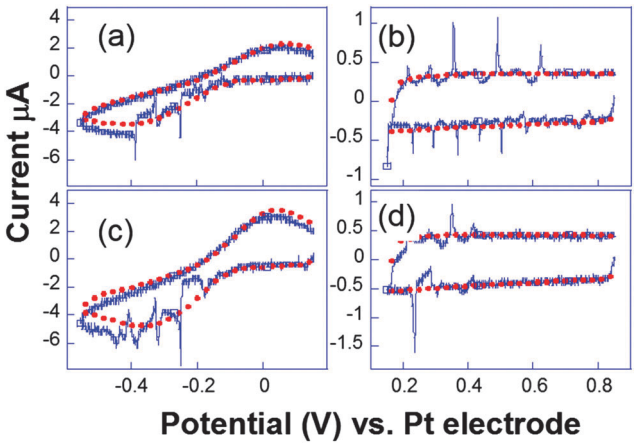

Fig. 9 Cyclic voltammograms recorded simultaneously ((a and c) and (b and d)) for two electrodes separated by 206 µm. Conditions: $K_3[Fe(CN)_6]$ (50 mM) in KNO_3 (0.1 M), horn-to-electrode distance 1 cm, electrode diameters 29 µm. Voltammograms under silent conditions (red) and subject to 8.9 W cm^{-2} insonation (blue) are represented. Adapted from ref. 67.

the back peak corresponding to the ferrocyanide reoxidation. This is proof that the diffusion layer structure returns to normal after a bubble collapse occurs. Experiments with a single microelectrode show thus that the cavitation activity is complex. Oscillations at harmonics of the driving frequency are observed with cyclic voltammetry experiments proving that the bubble is in the close vicinity of at least a part of the electrode. Due to the complexity of activity, the spatial dependence of a single cavitational event is difficult to assess since no theoretical model immediately allows easily relating the signal obtained to the space variables. For this purpose microelectrode arrays were used, because they allow a direct visualization of the spatial extension of the bubbles.[76] The chronoamperometric experiments presented above were repeated as before but the current was simultaneously recorded on different electrodes of the array. A typical array is shown in Fig. 10.

The appearance of cavitation peaks on the three electrodes is observed almost simultaneously in Fig. 10a, c and e. Since it is unlikely that two independent bubbles appear at around the same time on different electrodes and with the same peak shape and lifetime, it is inferred that the signals are induced by the same bubble. Analogous synchronous events could be recorded for distances as large as 0.8 mm using different electrode-to-electrode separations. Furthermore, in Fig. 10b, d and f, where the interelectrode distance was less than 5 µm, a signal is observed only on the central electrode. From geometrical considerations, we can estimate that the bubble size there is less than 40 µm. This behavior suggests that a wide distribution of bubble sizes is produced, including bubbles of sizes less than 40 µm. In experiments, the same type of signal with nearly the same current amplification was observed, suggesting that in these type of experiments (20 kHz, interfacial cavitation) the absence of a microjet, or if a microjet was present, it resulted ineffective in controlling the magnitude of the electrode signal, since different signals would be expected

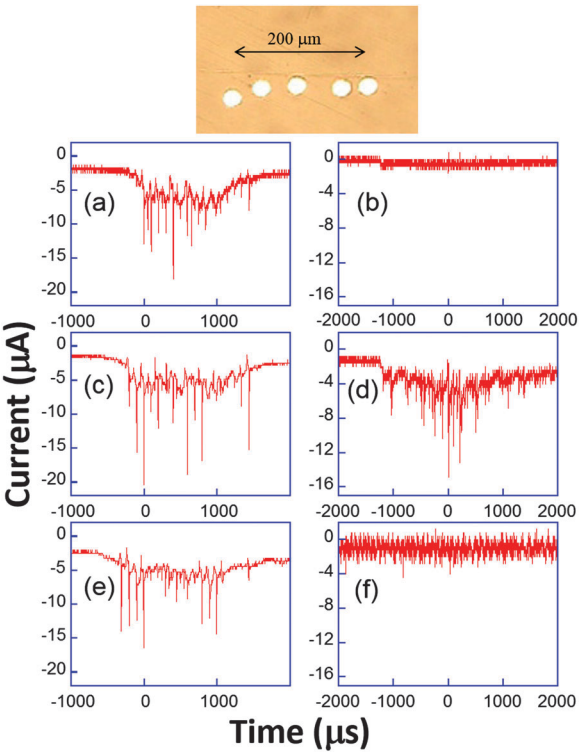

Fig. 10 Top: Example of microelectrode array. Bottom: Chronoamperometric current recorded simultaneously (a, c and e or b, d and f) on three electrodes using 50 mM $K_3[Fe(CN)_6]$ in aqueous KNO_3 (0.1 M). Adapted from ref. 67.

for electrode positions below the jet, below the toroidal bubble and outside the bubble. Furthermore, cyclic voltammetry experiments revealed that when cavitational activity is seen on two different electrodes, generally both show a depletion in the voltammogram (see Fig. 9) either in the faradaic current or in the background current. Since this depletion is attributed to blocking of the surface, bubbles are thus more likely to be hemispherical or flatter rather than spherical as often assumed prior to our study.

On the trace displayed in Fig. 11b a more quantitative interpretation was possible. Here, the chronoamperometric trace was obtained for the reduction of $[Ru(NH_3)_6]^{3+}$ in aqueous solution.

We considered a simple model of bubble implosion close to a surface as sketched in Fig. 11a. Firstly, we introduced the distance x_0 between the disk electrode and the bubble wall, and considered a potential sufficiently negative to ensure that the concentration C of electroactive species at the electrode surface was zero. Therefore, diffusion of the electroactive species from the solution ($C = C_0$) toward the electrode ($C = 0$) occurs. At time $t < 0$, the bubble grows and covers the electrode. Collapse occurs at $t = 0$ and bulk solution instantaneously replaces the bubble but the thin layer (TL) above the electrode x_0 is still fully electrolysed: the concentration of the electroactive species in TL and the current are then both zero. After the collapse, bulk solution instantaneously replaces the bubble above TL and diffusion of the electroactive compound inside TL occurs.

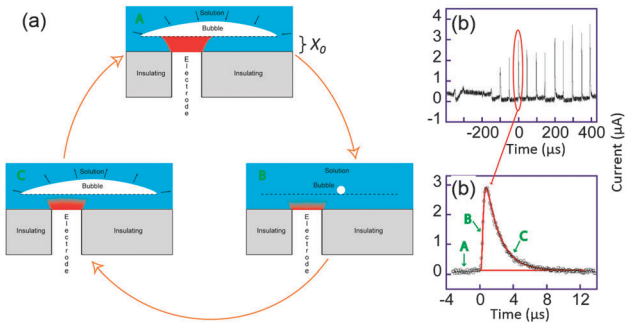

Fig. 11 (a) Sketch of bubble evolution near a surface. (b) Single bubble cavitation chronoamperometric current recorded for $[Ru(NH_3)_6]Cl_3$ (10 mM) in aqueous KNO_3 (0.1 M) under sonication at 20 kHz. Conditions: horn-to-electrode distance 7 mm, insonation power 8.9 W cm^{-2}, electrode diameter 32 μm. (c) Zoom on a single spike (circles) and simulation (line). For simplicity reduction currents are here positive. Adapted from ref. 68.

This model neglects macroscopic streaming as this has been shown to correspond to larger diffusion layers than are actually observed experimentally for the transient, as opposed to the steady-state response. After a time t_0, it is believed that the bubble expands again, thus recreating another thin layer of the same thickness x_0. The electrode is then blocked again and the current drops to zero within a time proportional to $x_0^2/(2D)$, where D is the diffusion coefficient of the redox system.

Theory based on this model was used to fit all the cavitation spikes shown in Fig. 11b. The peak height and width was matched with the working curve data. This allowed values of x_0 and t_0 be theoretically deduced.[68] Comparing the experimental voltammograms with the simulations gave a very good fit for several peaks whereas other peaks could not be described by the theory developed. The peaks for which the model was unsuccessful possibly resulted from a different bubble/electrode distance x_0 before and after the collapse, although x_0 would remain of the same order of magnitude in size. It is not unexpected to observe such variations under the conditions used, since the precise behaviour of the bubble results from a complex acoustic field influenced by the presence of neighbouring bubbles as well as by the local surface roughness. A large range of values for t_0 were obtained, which reveals that even in this apparent periodic signal a partially chaotic bubble behaviour exists. The experimental t_0 values suggest that most of the time the bubble covers the electrode, which is a similar conclusion to that of Leighton based on simulations.[77–79] Furthermore x_0 values were shown to range between 45 and 75 nm, which implies only small variations of x_0 over the whole chronoamperogram. These variations are consistent with the quasi steady-state current observed between the spikes. This current is due to a slow solution penetration in the bubble electrode gap that grows at velocities of *ca.* 1×10^{-4} m s^{-1}. The presence of a thin layer of a solution between the bubble wall and the surface could thus be established and quantified.

The deduced values of t_0 gave an average value of 0.2 μs. This gives an average minimum wall velocity ranging from 160 to 320 m s^{-1} depending on the bubbles' position.[77–79] Though the nanometric evolution of the interface can not be optically visualized, recording of the bubble size, shape and position as a function of time may be a first step to introduce more parameters in the model and unravel the complex behaviour of these fast evolving triple boundaries interfaces. Thanks to ultrafast electrochemistry, the effects of ultrasound irradiation could be rationalized which is of major importance in many fields of physics (for the example semi-conductor industry), chemistry and biology where ultrasonic bath treatment have become a standard operation.[69,70]

Pulse radiolysis coupled with transient electrochemistry

In molecular electrochemistry, the characteristic shape of the voltammogram and its evolution with the scan rate or concentration of reactants are determined by a subtle interplay between thermodynamic parameters such as the standard potentials and the kinetic rates of homogeneous or heterogeneous chemical reactions.[2] One strategy to extract the standard potentials is then to increase the scan rate until competing with the reaction of interest, which represents another advantage of ultrafast cyclic voltammetry. Ultrafast cyclic voltammetry nevertheless requires large enough concentrations to ensure a significant faradaic contribution (proportional to $\nu^{1/2}$) in comparison with the capacitive one (proportional to ν).[2,80] When not successful, redox catalysis may also be an interesting alternative, but again a full mechanistic scheme needs to be considered, and particularly the rate of product reactivity.[81]

Apart from electrochemical methods, pulse radiolysis has also demonstrated its advantages for deciphering mechanisms and measuring rate constants in homogeneous reactions. In this approach, a high energy electron pulse is sent through a solution containing the analyte. It induces breakdown of water and production of the so-called primary species, *i.e.* hydrogen radical $H^\bullet$, solvated electrons e_{aq}^- and hydroxyl radical $OH^\bullet$ (Scheme 1). These initial solution therefore contains both very reductive entities ($H^\bullet$, e_{aq}^-) but also very oxidative ones ($OH^\bullet$).[82]

With large excess of specific adjuvants, one can scavenge some species and switch the medium to either a reductive or oxidant one, and find conditions where after a few nano or microseconds, only one reaction dominates the evolution of the medium.[82,83] Usually, transient spectroscopy is used to follow the kinetics so that the temporal resolution of this techniques has followed the technological evolution of the laser systems.[84] Presently some systems reach a few picoseconds resolution, allowing the very initial aspects of radiolysis to be analyzed.[85] In fact, since a long time pulse radiolysis has provided the community a wide range of kinetics rate constants useful for

Scheme 1 Production of primary radicals by water radiolysis.

many communities including the electrochemical one.[82] Usually, only micromolar concentrations of radicals are created, so that fast bimolecular decays may still be intercepted at the electrode.

We very recently reactivated a coupling proposed initially by Henglein *et al.* in the seventies but then abandoned.[86] It happens to be very complementary to the spectroscopic approach. Here, an electrode is placed on the path of the electron beam and set at a constant potential. The radicals created in solution by the electron beam are thus intercepted at the electrode. We present below our results onto methylviologen, a typical intermediate used both in electrochemistry and spectroscopy, and those relying to guanosine, in the framework of oxidative stress.

Our experiments were run on the ELYSE platform in Orsay. This electron accelerator provides electron pulses of 7–8 MeV energy that are thus not blocked by the electrode. Electrons are extracted from a Cs_2Te photocathode by a femtosecond laser.[84] Simultaneously, transient spectra can be recorded with a streak camera with a temporal resolution from a few picoseconds to a few milliseconds. To perform electrochemical acquisitions, we placed a gold ball electrode in the path of the electrons, whereas the counter and reference electrodes were placed outside the electron beam as sketched in Fig. 12a. The current can then be recorded at potentials for which the faradaic current is negligible when radiolysis does not occur.

Fig. 12c presents the transient obtained for a solution containing 1 mM methylviologen (MV^{2+}), 0.35 M of Na_2SO_4 as supporting electrolyte and 50 mM of isopropanol. Isopropanol is used to scavenge $OH^{\bullet}$ according to the scheme provided in Fig. 12b.[87]

MV^{2+} was then reduced both by the solvated electrons and by the isopropanol radical. When the cell was placed a few centimeters away from the electron beam, a large parasitic signal was obtained. In comparison to previous experiments performed with nanosecond pulses, we believe that the concentrated electron beam induces an electromagnetic destabilization of the potentiostat loop. Fortunately, this spike can be subtracted so as to recover only the faradaic signal. Since $MV^{\bullet+}$ is a stable radical, a diffusion limited current with a $t^{-1/2}$ dependence corresponding to reoxidation of $MV^{\bullet+}$ into MV^{2+} was observed (*cf.* Fig. 12c). This allowed to determine the concentration of radicals created (1.7×10^{-5} μM), in perfect agreement with the spectroscopic measurements. This first experiment onto a well-behaved probe validated our approach.

The situation is much more complex when unstable radicals are created. In solution, bimolecular decays are then usually observed. But in addition, these unstable species may undergo oxidation and reduction at the electrode simultaneously. This is reminiscent of the observation that excited states created by light absorption are both better donor and better acceptors than the fundamental one. In electrochemistry, these systems often undergo ECE type mechanisms, the intermediate produced after the first electron transfer being unstable. In this context, in our methodology, the first electron transfer is induced by radiolysis, which allows to study the second one at potentials where the first one does not occur. With this idea but a different experimental approach, Saveant and Hapiot could already measure the redox potentials of several intermediates by ejecting electrons from the electrode with a laser pulse.[88–90]

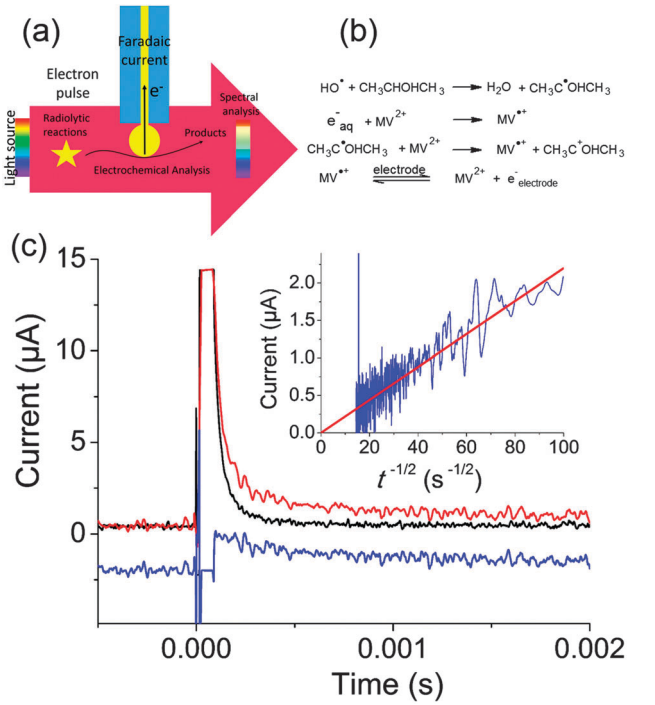

Fig. 12 (a) Principle of electrochemical detection of intermediates created by pulse radiolysis. (b) Chemical reactions leading to production of $MV^{\bullet+}$. (c) Transient electrochemical signal observed when a solution containing 1 mM MV^{2+}, 0.35 M Na_2SO_4 and 50 mM isopropanol was irradiated with a pulse of 25 Gy. Black: parasitic signal obtained when the electrode is placed outside the beam. Red: electrochemical signal obtained when the electrode is positioned on the electron trajectory. Blue: faradaic signal obtained by subtraction (−2 μA offset was applied for clarity) Inset: *I versus* $t^{-1/2}$ and linear fit of the faradaic signal. Adapted from ref. 88.

Very often, electrochemical investigations in water for biological intermediates are extremely difficult to undertake. Indeed, several electrochemical and chemical steps occur, and the products formed adsorb onto the electrode for the millimolar or submillimolar concentrations often used in electrochemistry to yield sufficient current signals. The main consequence is that most of the publications concern analytical determination often using modified electrodes, but without deep study on the mechanism. On the other hand, in biological reactions the range of concentrations involved is often far below the millimolar range, which stimulated us further to explore the reactivity of biological intermediates by pulse radiolysis combined with electrochemistry.

Within this framework, we recently explored the electrochemical properties of the guanosine and guanosine monophosphate radicals (both labeled G(–H)$^{\bullet}$ in the following) created by $Br_2^{\bullet-}$, a one electron oxidant.[91] Here, the solvated electrons are quenched by N_2O so as to switch to oxidative conditions and the reaction scheme follows eqn (14–18) (Scheme 2).

$$N_2O + e^-_{aq} + H_2O \longrightarrow HO^\bullet + OH^- + N_2 \quad (14)$$

$$Br^- + HO^\bullet \longrightarrow BrOH^{\bullet -} \quad (15)$$

$$BrOH^{\bullet -} + Br^- \longrightarrow Br_2^{\bullet -} + OH^- \quad (16)$$

$$Br_2^{\bullet -} + G \longrightarrow G^{\bullet +} + 2Br^- \quad (17)$$

$$G^{\bullet +} \longrightarrow G(-H)^\bullet + H^+ \quad (18)$$

Scheme 2 Mechanism of guanosine radical production.

After 200 μs, the solution contains only G(–H)•. Previous studies by pulse radiolysis determined an apparent redox potential of $E^{0'}_{red} = 1.29$ V/SHE for the system G(–H)•/G at pH 7.[92] In addition, G(–H)• can react with either oxidants (to probably lead to 8-oxoguanosine) or reductants (to give back G), which was termed the redox ambivalence.[93]

At the electrode, this ambivalence is balanced by the electrode potential, and the current transients displayed in Fig. 13 display a progressive shift from reduction to oxidation. At low potentials, the reduction predominates, so that the dimerization rate of the radical is accurately determined: $k_{SO} = 1.1 \pm 0.3 \times 10^7$ M^{-1} s^{-1} for guanosine monophosphate and $3 \pm 1 \times 10^7$ M^{-1} s^{-1} for guanosine. At intermediate potentials, the competition is regulated both by thermodynamic parameters, the standard potentials corresponding to oxidation or reduction of the radical, and by kinetic ones, the heterogeneous rate constants of these reactions. In our case, since the oxidation potential $E^{0'}_{red}$ was known from the literature, we could determine $E^{0'}_{ox} = 0.37$ V/SHE. In addition, it has to be underlined that since the electrode potential was poised far from the standard potentials, we observed an effect involving a quadratic dependence of the activation energy *versus* the overpotential as included in the integral of eqn (7). This allowed to deduce a reorganization energy of 0.9 eV, supposed equal for oxidation or reduction.

Here, pulse radiolysis then offered the possibility to generate micromolar concentrations of intermediate that can then undergo electron transfer at the electrode. The study of the radical is then not correlated to their production, unlike in classical electrochemical methods. Guanosine demonstrate the interest of the approach for biological systems, but the methodology will also be extended to other fields in the future.

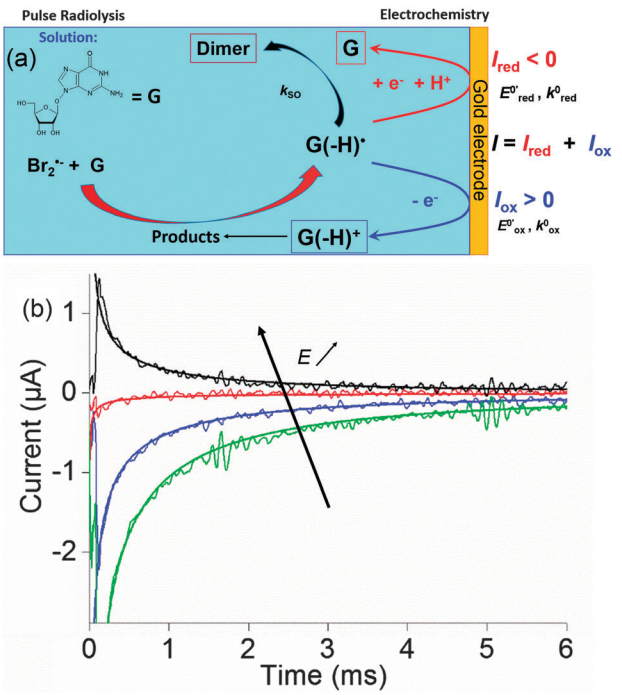

Fig. 13 (a) Scheme of guanosine or guanosinemonophosphate reactivity in solution. Reaction in solution provides a dimer while the radical may also be oxidized or reduced at the electrode surface. (b) Faradaic current transients and simulations observed for guanosinemonophosphate at 103 mV (green), 582 mV (blue), 621 mV (red) and 651 mV (black) *vs.* AgCl/Ag. Parameters for the simulations: $E^{0'}_{red} = 1.09$ V *vs.* AgCl/Ag, $E^{0'}_{ox} = 0.17$ V *vs.* AgCl/Ag, $k_{SO} = 1.1 \times 10^7$ M^{-1} s^{-1}, $k^0_{ox} = k^0_{red} = 1$ cm s^{-1}, $\lambda_{ox} = \lambda_{red} = 0.9$ eV. Dose 38 Gy per pulse, corresponding to an initial G(–H)• concentration of 28 μM. Adapted from ref. 92.

Conclusions

The examples presented above underline the advantages of transient measurements in electrochemistry. In this respect, micrometric electrodes are required to minimize ohmic losses and provide a low time constant. Extremely rapid electron transfer in molecular wires or in macromolecules may be probed in this way, providing necessary information in view of their potential incorporation in molecular electronic devices. An ultrafast potentiostat may also be used to observe phenomena induced by a non-electrochemical perturbation. Herein, a great precision was obtained about the acoustic bubbles movements evolving a few nanometers above the electrodes. On the other hand, though heavy to implement, coupling electrochemistry with pulse radiolysis represents a powerful approach to study mechanisms in water at very low concentrations relevant to biological media.

We hope that this review convinced the reader of fast electrochemistry usefulness in unravelling original systems not accessible by other methodologies.

Acknowledgements

This work was supported by ANR (project Radiolyse et Analyse Dynamique par Electrochimie, JCJC 0810), the CNRS Exchange of researchers program, the Universite Pierre et Marie Curie, the National Natural Science Foundation of China (No. 21573198 and 21273204) and Zhejiang Provincial Natural Science Foundation of China (No. LR15B030002).

Notes and references

1 A. J. Bard and L. R. Faulkner, *Electrochemical Methods*, Wiley, New York, 2001.
2 J.-M. Saveant, *Elements Molecular and Biomolecular Electrochemistry*, John Wiley and Son, Hoboken, New Jersey, 1st edn, 2006.

3 N. V. Rees, O. V. Klymenko, E. Maisonhaute, B. A. Coles and R. G. Compton, *J. Electroanal. Chem.*, 2003, **542**, 23–32.
4 J. J. Watkins, J. Y. Chen, H. S. White, H. D. Abruna, E. Maisonhaute and C. Amatore, *Anal. Chem.*, 2003, **75**, 3962–3971.
5 *Scanning Electrochemical Microscopy*, ed. A. J. Bard and M. V. Mirkin, Taylor & Francis, Boca Raton, FL, 2nd edn, 2012.
6 F. R. F. Fan and A. J. Bard, *Science*, 1995, **267**, 871–874.
7 R. Forster and L. Faulkner, *J. Am. Chem. Soc.*, 1994, **116**, 5453–5461.
8 N. V. Rees, C. E. Banks and R. G. Compton, *J. Phys. Chem. B*, 2004, **108**, 18391–18394.
9 M. E. Orazem and B. Tribollet, *Electrochemical Impedance Spectroscopy*, John Wiley & Sons, Hoboken, New Jersey, 2008.
10 C. Amatore and E. Maisonhaute, *Anal. Chem.*, 2005, **77**, 303A–311A.
11 C. Amatore, S. Arbault, E. Maisonhaute, S. Szunerits and L. Thouin, in *Trends In Molecular Electrochemistry*, ed. J. L. Pombeiro and C. Amatore, Fontis Media, Lausanne, 2004, pp. 385–411.
12 C. Amatore, C. Lefrou and F. Pfluger, *J. Electroanal. Chem.*, 1989, **270**, 43–59.
13 C. Amatore and C. Lefrou, *J. Electroanal. Chem.*, 1992, **324**, 33–58.
14 C. P. Andrieux, D. Garreau, P. Hapiot and J. M. Saveant, *J. Electroanal. Chem.*, 1988, **248**, 447–450.
15 C. P. Andrieux, P. Hapiot and J. M. Saveant, *Electroanalysis*, 1990, **2**, 183–193.
16 D. Garreau, P. Hapiot and J. M. Saveant, *J. Electroanal. Chem.*, 1990, **281**, 73–83.
17 R. M. Wightman and D. O. Wipf, *Acc. Chem. Res.*, 1990, **23**, 64–70.
18 D. O. Wipf and R. M. Wightman, *Anal. Chem.*, 1988, **60**, 2460–2464.
19 D. O. Wipf, E. W. Kristensen, M. R. Deakin and R. M. Wightman, *Anal. Chem.*, 1988, **60**, 306–310.
20 C. Amatore, E. Maisonhaute and G. Simonneau, *J. Electroanal. Chem.*, 2000, **486**, 141–155.
21 C. Amatore, E. Maisonhaute and G. Simonneau, *Electrochem. Commun.*, 2000, **2**, 81–84.
22 P. Fortgang, C. Amatore, E. Maisonhaute and B. Schollhorn, *Electrochem. Commun.*, 2010, **12**, 897–900.
23 C. Arrigoni, G. Schull, D. Bleger, L. Douillard, C. Fiorini-Debuisschert, F. Mathevet, D. Kreher, A. J. Attias and F. Charra, *J. Phys. Chem. Lett.*, 2010, **1**, 190–194.
24 P. Aubertin, M. Aissa, N. Raouafi, S. Joiret, A. Courty and E. Maisonhaute, *Nano Res.*, 2015, **8**, 1615–1626.
25 S. S. Isied, M. Y. Ogawa and J. F. Wishart, *Chem. Rev.*, 1992, **92**, 381–394.
26 J. C. Genereux and J. K. Barton, *Chem. Rev.*, 2010, **110**, 1642–1662.
27 D. M. Adams, L. Brus, C. E. D. Chidsey, S. Creager, C. Creutz, C. R. Kagan, P. V. Kamat, M. Lieberman, S. Lindsay, R. A. Marcus, R. M. Metzger, M. E. Michel-Beyerle, J. R. Miller, M. D. Newton, D. R. Rolison, O. Sankey, K. S. Schanze, J. Yardley and X. Y. Zhu, *J. Phys. Chem. B*, 2003, **107**, 6668–6697.
28 R. A. Marcus, *J. Chem. Phys.*, 1965, **43**, 679.
29 C. E. D. Chidsey, *Science*, 1991, **251**, 919–922.
30 E. Laborda, M. C. Henstridge, C. Batchelor-McAuley and R. G. Compton, *Chem. Soc. Rev.*, 2013, **42**, 4894–4905.
31 H. D. Sikes, J. F. Smalley, S. P. Dudek, A. R. Cook, M. D. Newton, C. E. D. Chidsey and S. W. Feldberg, *Science*, 2001, **291**, 1519–1523.
32 R. J. Nichols, W. Haiss, S. J. Higgins, E. Leary, S. Martin and D. Bethell, *Phys. Chem. Chem. Phys.*, 2010, **12**, 2801–2815.
33 B. Q. Xu and N. J. Tao, *Science*, 2003, **301**, 1221–1223.
34 W. Haiss, T. Albrecht, H. van Zalinge, S. J. Higgins, D. Bethell, H. Hobenreich, D. J. Schiffrin, R. J. Nichols, A. M. Kuznetsov, J. Zhang, Q. Chi and J. Ulstrup, *J. Phys. Chem. B*, 2007, **111**, 6703–6712.
35 B. Q. Xu, X. Y. Xiao, X. M. Yang, L. Zang and N. J. Tao, *J. Am. Chem. Soc.*, 2005, **127**, 2386–2387.
36 D.-F. Li, J.-C. Mao, D.-L. Chen, F. Chen, H. Ze-Wen, X.-Y. Zhou, Y.-H. Wang, X.-S. Zhou, Z.-J. Niu and E. Maisonhaute, *Electrochim. Acta*, 2015, **174**, 340–344.
37 L. Venkataraman, J. E. Klare, C. Nuckolls, M. S. Hybertsen and M. L. Steigerwald, *Nature*, 2006, **442**, 904–907.
38 M. C. Traub, B. S. Brunschwig and N. S. Lewis, *J. Phys. Chem. B*, 2007, **111**, 6676–6683.
39 A. Nitzan, *J. Phys. Chem. A*, 2001, **105**, 2677–2679.
40 A. Migliore and A. Nitzan, *Electrochim. Acta*, 2015, **160**, 363–375.
41 T. Albrecht, K. Moth-Poulsen, J. B. Christensen, A. Guckian, T. Bjornholm, J. G. Vos and J. Ulstrup, *Faraday Discuss.*, 2006, **131**, 265–279.
42 J. Zhang, A. M. Kuznetsov, I. G. Medvedev, Q. Chi, T. Albrecht, P. S. Jensen and J. Ulstrup, *Chem. Rev.*, 2008, **108**, 2737–2791.
43 E. Leary, S. J. Higgins, H. van Zalinge, W. Haiss, R. J. Nichols, S. Nygaard, J. O. Jeppesen and J. Ulstrup, *J. Am. Chem. Soc.*, 2008, **130**, 12204–12205.
44 N. J. Kay, S. J. Higgins, J. O. Jeppesen, E. Leary, J. Lycoops, J. Ulstrup and R. J. Nichols, *J. Am. Chem. Soc.*, 2012, **134**, 16817–16826.
45 X. S. Zhou, L. Liu, P. Fortgang, A. S. Lefevre, A. Serra-Muns, N. Raouafi, C. Amatore, B. W. Mao, E. Maisonhaute and B. Schollhorn, *J. Am. Chem. Soc.*, 2011, **133**, 7509–7516.
46 X. L. Li, J. He, J. Hihath, B. Q. Xu, S. M. Lindsay and N. J. Tao, *J. Am. Chem. Soc.*, 2006, **128**, 2135–2141.
47 W. Haiss, S. Martin, E. Leary, H. van Zalinge, S. J. Higgins, L. Bouffier and R. J. Nichols, *J. Phys. Chem. C*, 2009, **113**, 5823–5833.
48 C. Li, I. Pobelov, T. Wandlowski, A. Bagrets, A. Arnold and F. Evers, *J. Am. Chem. Soc.*, 2008, **130**, 318–326.
49 J. H. Tian, Y. Yang, X. S. Zhou, B. Schollhorn, E. Maisonhaute, Z. B. Chen, F. Z. Yang, Y. Chen, C. Amatore, B. W. Mao and Z. Q. Tian, *ChemPhysChem*, 2010, **11**, 2745–2755.
50 C. Amatore, E. Maisonhaute, B. Schollhorn and J. Wadhawan, *ChemPhysChem*, 2007, **8**, 1321–1329.
51 W. Haiss, H. van Zalinge, D. Bethell, J. Ulstrup, D. J. Schiffrin and R. J. Nichols, *Faraday Discuss.*, 2006, **131**, 253–264.
52 M. Kamenetska, S. Y. Quek, A. C. Whalley, M. L. Steigerwald, H. J. Choi, S. G. Louie, C. Nuckolls, M. S. Hybertsen, J. B. Neaton and L. Venkataraman, *J. Am. Chem. Soc.*, 2010, **132**, 6817–6821.
53 C. Leger and P. Bertrand, *Chem. Rev.*, 2008, **108**, 2379–2438.
54 B. Giese, *Annu. Rev. Biochem.*, 2002, **71**, 51–70.
55 H. Dahms, *J. Phys. Chem.*, 1968, **72**, 362.
56 I. Ruff and I. Korosiod, *Inorg. Chem.*, 1970, **9**, 186.
57 D. N. Blauch and J. M. Saveant, *J. Am. Chem. Soc.*, 1992, **114**, 3323–3332.
58 C. Amatore, Y. Bouret, E. Maisonhaute, J. I. Goldsmith and H. D. Abruna, *ChemPhysChem*, 2001, **2**, 130–134.
59 C. Amatore, Y. Bouret, E. Maisonhaute, J. I. Goldsmith and H. D. Abruna, *Chem. – Eur. J.*, 2001, **7**, 2206–2226.
60 J. A. Camerano, M. A. Casado, U. Hahn, J. F. Nierengarten, E. Maisonhaute and C. Amatore, *New J. Chem.*, 2007, **31**, 1395–1399.
61 U. Hahn, E. Maisonhaute, C. Amatore and J. F. Nierengarten, *Angew. Chem., Int. Ed.*, 2007, **46**, 951–954.
62 P. Fortgang, E. Maisonhaute, C. Amatore, B. Delavaux-Nicot, J. Iehl and J. F. Nierengarten, *Angew. Chem., Int. Ed.*, 2011, **50**, 2364–2367.
63 C. Amatore, F. Grun and E. Maisonhaute, *Angew. Chem., Int. Ed.*, 2003, **42**, 4944–4947.
64 M. Erard, A. Fredj, H. Pasquier, D. B. Beltolngar, Y. Bousmah, V. Derrien, P. Vincent and F. Merola, *Mol. BioSyst.*, 2013, **9**, 258–267.
65 F. Merola, A. Fredj, D. B. Betolngar, C. Ziegler, M. Erard and H. Pasquier, *Biotechnol. J.*, 2014, **9**, 180–191.
66 R. G. Compton, F. Marken and T. O. Rebbitt, *Chem. Commun.*, 1996, 1017–1018.
67 E. Maisonhaute, P. C. White and R. G. Compton, *J. Phys. Chem. B*, 2001, **105**, 12087–12091.
68 E. Maisonhaute, B. A. Brookes and R. G. Compton, *J. Phys. Chem. B*, 2002, **106**, 3166–3172.
69 E. Maisonhaute, F. J. Del Campo and R. G. Compton, *Ultrason. Sonochem.*, 2002, **9**, 275–283.
70 E. Maisonhaute, C. Prado, P. C. White and R. G. Compton, *Ultrason. Sonochem.*, 2002, **9**, 297–303.
71 F. J. Del Campo, E. Maisonhaute, R. G. Compton, F. Marken and A. Aldaz, *J. Electroanal. Chem.*, 2001, **506**, 170–177.
72 R. G. Compton, J. C. Eklund and F. Marken, *Electroanalysis*, 1997, **9**, 509–522.
73 L. A. Crum, *J. Phys.*, 1979, **11**, C8–285.
74 A. Philipp and W. Lauterborn, *J. Fluid Mech.*, 1998, **361**, 75–116.
75 P. R. Birkin and S. SilvaMartinez, *J. Electroanal. Chem.*, 1996, **416**, 127–138.
76 P. R. Birkin, D. G. Offin and T. G. Leighton, *Electrochem. Commun.*, 2004, **6**, 1174–1179.
77 T. G. Leighton, *Ultrasonics*, 1989, **27**, 50–53.
78 T. G. Leighton, *The Acoustic Bubble*, Academic Press, 1994.
79 T. G. Leighton, A. J. Walton and J. E. Field, *Ultrasonics*, 1989, **27**, 370–373.
80 C. Amatore, G. Farsang, E. Maisonhaute and P. Simon, *J. Electroanal. Chem.*, 1999, **462**, 55–62.

81 A. Et Taouil, E. Brun, P. Duchambon, Y. Blouquit, M. Gilles, E. Maisonhaute and C. Sicard-Roselli, *Phys. Chem. Chem. Phys.*, 2014, **16**, 24493–24498.
82 P. Wardman and A. B. Ross, *Free Radical Biol. Med.*, 1991, **10**, 243–247.
83 E. Sutter, K. Jungjohann, S. Bliznakov, A. Courty, E. Maisonhaute, S. Tenney and P. Sutter, *Nat. Commun.*, 2014, **5**, 4946.
84 J. L. Marignier, V. de Waele, H. Monard, F. Gobert, J. P. Larbre, A. Demarque, M. Mostafavi and J. Belloni, *Radiat. Phys. Chem.*, 2006, **75**, 1024–1033.
85 A. Balcerzyk, U. Schmidhammer, G. Horne, F. Wang, J. Ma, S. M. Pimblott, A. de la Lande and M. Mostafavi, *J. Phys. Chem. B*, 2015, **119**, 10096–10101.
86 A. Henglein, in *Electroanalytical Chemistry – A Series of Advances*, ed. A. J. Bard, Marcel Dekker, New York, 1976, vol. 9, pp. 163–245.
87 M. S. Alam, E. Maisonhaute, D. Rose, A. Demarque, J. P. Larbre, J. L. Marignier and M. Mostafavi, *Electrochem. Commun.*, 2013, **35**, 149–151.
88 J. Gonzalez, P. Hapiot, V. Konovalov and J. M. Saveant, *J. Electroanal. Chem.*, 1999, **463**, 157–189.
89 P. F. Hapiot, L. D. Kispert, V. V. Konovalov and J. M. Saveant, *J. Am. Chem. Soc.*, 2001, **123**, 6669–6677.
90 C. P. Andrieux, J. Gamby, P. Hapiot and J. M. Saveant, *J. Am. Chem. Soc.*, 2003, **125**, 10119–10124.
91 A. Latus, M. S. Alam, M. Mostafavi, J. L. Marignier and E. Maisonhaute, *Chem. Commun.*, 2015, **51**, 9089–9092.
92 S. Steenken and S. V. Jovanovic, *J. Am. Chem. Soc.*, 1997, **119**, 617–618.
93 P. O'Neill and P. W. Chapman, *Int. J. Radiat. Biol.*, 1985, **47**, 71–80.